EXPERIMENT NO. 6

INVESTIGATION OF THE DYNAMICS OF A BEAM STRUCTURE

Submitted by:

JANE P. DOE

AEROSPACE AND OCEAN ENGINEERING DEPARTMENT

VIRGINIA POLYTECHNIC INSTITUTE AND STATE UNIVERSITY

BLACKSBURG, VIRGINIA

15 JANUARY 2006

EXPERIMENT PERFORMED 13 JANUARY 2006

LAB INSTRUCTOR: STEVEN R. EDWARDS

Honor Pledge:
By electronically submitting this report I pledge that I have neither given nor received unauthorized assistance on this assignment.

123456789	1/15/07
Student Number	Date

1. INTRODUCTION

The aims of this study are:

1. To determine the parameters governing the motion of a single degree of freedom beam structure using measurements of its response to sinusoidal forcing.
2. To evaluate two strategies for determining the viscous damping of the structure.
3. To compare results with nominal values of parameters given by Hallauer and Devenport (2006).

These aims were achieved by performing measurements and analysis on a laboratory structure of the type shown in Figure 1. The theoretical background of such structures is summarized below.

In general, any single-degree of freedom system can be thought of as being equivalent to the combination of a mass, a connected spring and a dashpot, as shown schematically in Figure 2. To determine the response of such a system it is necessary to analyze its motion. Balancing the forces acting on the mass, *m*, in Figure 2 gives the equation of motion:

$$m\ddot{x} + b\dot{x} + kx = f(t) \tag{1}$$

where k is the spring constant, b is the damping coefficient and $f(t)$ is the applied force. The parameters m, b and k completely define the dynamics of the structure. Solving equation (1) for a sinusoidally fluctuating force at an angular frequency, ω, it is found that the amplitude of the motion, x_m , and the amplitude of the force that produces it, f_m , are related as:

$$\frac{x_m}{f_m} = \frac{1}{\sqrt{(k - m\omega^2)^2 + b^2\omega^2}} \equiv g(\omega) \tag{2}$$

See, for example, Ogata (1998). This ratio is referred to as the dynamic flexibility, given here the symbol, *g*. The phase lag between the motion and force ψ_m is

$$\psi_m = \arctan\left(-\frac{b}{k - m\omega^2}\right) \tag{3}$$

It is possible to design an experiment to determine the parameters *m, b* and *k* through measurements of the dynamic flexibility and phase lag and the use of equations (2) and (3). For example, the spring stiffness, *k*, can be inferred from a measure of the dynamic flexibility at zero or very low frequency, since *g*(0)=1/*k*. The system mass, *m*, can then be determined by measuring the natural frequency, ω_n , since $\omega_n = \sqrt{k/m}$ and thus

$$m = \omega_n^2 / k \tag{4}$$

The natural frequency can be identified using the fact that the phase is -90 degrees here.

Two straightforward methods for determining the damping, *b*, present themselves. We can either measure the dynamic flexibility at the natural frequency

$$g(\omega_n) = 1/(b\omega_n) \tag{5}$$

or measure the resonant frequency

$$\omega_r = \omega_n\sqrt{1 + \tfrac{1}{2}b^2/k} \tag{6}$$

at which the dynamic flexibility is a maximum.

In the present study these approaches are used to measure the parameters of a dynamical system. Uncertainty analysis is also used to reveal the best method for determining the damping. The remainder of this report is organized as follows. The following section includes a detailed description of the structure, the experimental instrumentation and procedures. Results are then presented in Section 3 along with

uncertainty estimates and a comparison of the measured parameters with nominal values. Finally conclusions are drawn. Most importantly we find that damping coefficient can be determined with reasonable accuracy from the dynamic flexibility at the natural frequency. We also find the nominal mass of the structure to be in error by at least 26%

2. APPARATUS AND TECHNIQUES

2.1 Test Structure

The test structure (Figures 3 and 4) is mounted inside a wooden frame. A large aluminum block firmly attached to the frame serves as a fixed support for the structure. Two parallel aluminum beams, cantilevered from the block, support a rigid mass that is free to vibrate in the *x* direction as illustrated in Figure 1. The beams are also cantilevered at the mass preventing any rotation of the mass as it moves. The rectangular cross section of the beams also prevents any out-of-plane vibration. The beams and mass are made from aluminum.

At rest, the distance between the block and mass, and thus the free length of each beam, is 305±0.8 mm. The cross section of each beam is 76.6×5.4 mm with an uncertainty of 0.05 mms The rigid mass, including embedded portions of the beams and their attachment brackets, has a total length of 152.3±0.05 mm, a width of 62.9±0.05 mm and depth of 76.6±0.05 mm. Attached to one side of the mass is an Airport dashpot (type not recorded), and to the other side the coil of a solenoid-type electromechanical shaker (type not available), as shown in Figure 3.

Values given in the AOE 3054 Course Manual (Hallauer and Devenport, 2006) for the beam stiffness and length imply a combined spring constant, *k*, for the two beams

of 7636 N/m. The manual also gives the rigid mass (including mass of the shaker coil, dashpot piston, embedded portions of the beams and mounting brackets) as 0.726 kg. Technically the value of the mass, *m*, appearing in the equation of motion of the structure should also include contributions from the two beams but, as discussed by Hallauer and Devenport (2006), these were expected to be small. Finally the manual includes the nominal amplitude and phase response in graphical form, these charts indicating a natural frequency of close to 16 Hz.

For all measurements the wooden frame containing the beam structure was placed on the laboratory floor, this being the lowest floor level in the building. This minimized contamination of the response measurements through building vibrations, and removed the possibility of the structural dynamics coupling with a laboratory bench. Care was taken to keep cables and other obstructions clear of the beam system to avoid mechanical interference.

2.2 Excitation system

The structure was excited using fluctuating forces applied through the shaker coil attached to one side of the rigid mass, Figure 5. The coil moves inside, but does not touch, a permanent magnet fixed to the wooden frame. Force is generated between the magnet and coil when a current is passed through the coil.

A Tektronix function generator, type CFG250, was use to generate the sinusoidal excitation signal which was delivered to the shaker through a generic power amplifier. The calibration of the power amplifier/shaker combination, shown in Figure 6, indicates that it generates close to 0.363 N/V (0.0817 lb/V). Force amplitudes were inferred from

this calibration factor and measured voltage amplitudes. Both a Tektronix multimeter (type CDM 250) and oscilloscope (type 2205) were available to measure voltage amplitudes. However, after initial testing only the latter was used due to frequency limitations on the multimeter. A Beckman UC10A counter was used to measure the frequency of excitation signals. A schematic of the excitation system is shown in Figure 7.

For the low frequency measurements used to determine the spring constant the excitation amplitude was set at 2 V and the coil only energized for limited times in order to avoid overheating. For the measurements around the response peak (natural and resonant frequency) the excitation amplitude was set so as to produce a response amplitude of 2 V. Uncertainty in excitation voltage amplitude measured with the scope was typically $1/20^{th}$ of a division, corresponding to 0.025 V for the low frequency measurements and 0.005 V for the tests around the response peak. These values are equivalent to uncertainties in force amplitude, f_m , of 0.0091 N and 0.0018 N respectively. For frequency measurements the gate time on the Beckman counter was set to 10 seconds, giving a frequency resolution (and apparent uncertainty) of 0.1 Hz.

2.3 Response system

The instantaneous position of the rigid mass was sensed using a proximeter system. The system uses a non-contact probe (Bentley Nevada Corporation type 300-00-00-30-36-02) mounted on an arm to the fixed wooden frame, Figure 8. The probe, operated using an Bentley Nevada type 3120-8400-300 proximeter was used to sense the

distance to small steel target mounted to the rigid mass. A Tecktronix CPS250 power supply was used to provide the -18 V power required by the proximeter.

The calibration of the proximeter system, in terms of the voltage it outputs as a function of the distance between the probe and target, is shown in Figure 9. The probe has a range of some 180 mils (about 4.5 mm), but is most linear for distances around 70 mils (about 1.8 mm) corresponding to output voltages around -6 V. The calibration slope here corresponds to 4173 V/m. The probe position relative to the target was adjusted to give –6 V output with no force applied to the rigid mass, so as to take advantage of this linear range. During testing, the amplitude of the proximeter output voltage fluctuation, and thus the amplitude of the beam vibration, was measured using the Tektronix 2205 oscilloscope. The uncertainty of these measurements was 0.025 V for the low frequency tests and about 0.2 V for the tests around the response peak, corresponding to uncertainties in x_m of 6.0×10^{-6} m and 4.8×10^{-5} m respectively. The much larger uncertainty around the response peak was the result of slow drifting of the amplitude here, over a timescale of some 20 to 30 seconds. A Lissajous figure, with the oscilloscope in XY mode, was used to judge when the phase lag was -90 degrees and thus determine the natural frequency of the system. The accuracy of the natural frequency determined using this method was limited to 0.1 Hz by the resolution of the counter. A schematic of the response system is shown in Figure 10.

2.4 Other items of equipment

A digital camera (Cannon A510) was used the photograph the instrumentation and set up. A steel ruler (1/16" divisions) and caliper (1/1000" resolution) were used to measure dimensions of the various components of the beam system.

3. RESULTS AND DISCUSSION

3.1 Low frequency measurements

Measurements to determine the spring constant k of the structure, using the low-frequency asymptote of Equation (2), $g(0)=1/k$, were performed by exciting the structure at frequencies much less than the expected natural frequency of 16 Hz. Results for frequencies between 0.6 and 3 Hz, are listed in Table 1. The table includes measurements of the amplitude of the applied force, f_m , and of the resulting beam displacement, x_m , as well as the dynamic flexibility calculated by dividing these values. Figure 11 shows a plot of the dynamic flexibility plotted vs. frequency.

Table 1 Response of the structure (in terms of displacement amplitude, x_m) to low-frequency sinusoidal forcing (of amplitude f_m), and implied values of the dynamic flexibility, g.

Frequency (Hz)	f_m (N)	x_m (m)	g (m/N)
3.0	0.727	0.0001198	0.000165
2.1	0.727	0.0001078	0.000148
1.0	0.727	0.0000958	0.000132
0.6	0.727	0.0000958	0.000132

The measurements do show some variation in the dynamic flexibility with frequency, which decreases from 0.000165 m/M at 3.0 Hz to 0.00132 m/N at 1.0 Hz. However further lowering of the frequency to 0.6 Hz makes no difference to the measured flexibility, suggesting that the low-frequency asymptote has been reached. The

value of $g(0)$ is therefore taken to be 0.132 m/N, implying a spring stiffness, k, of 7583 N/m. The uncertainty in this measurement, calculated in the appendix, is 450 N/m or about 6%. The present results therefore confirm the nominal spring stiffness given by Hallauer and Devenport (2006) of 7636 N/m.

3.2 Measurements around the response peak

The effective mass, m, of the structure was estimated by using using a Lissajous figure to determine the frequency at which the phase between excitation and response was -90 degrees, i.e. the natural frequency, ω_n. The mass was then determined from this frequency and the measured spring constant using equation (4). Estimates of the damping constant, b, were obtained both from the measured dynamic flexibility at the natural frequency and from measuring the resonant frequency, with appropriate use of Equations (5) and (6). An important objective of this test was to compare these two methods.

Table 2 Measurements of the natural and resonant frequencies and of dynamic flexibility, g, at the natural frequency, along with implied values of the mass, m, and damping constant, b.

	Frequency (Hz)	f_m (N)	x_m (m)	g (m/N)	k (N/m) Table 1	m (kg) eqn. 4	b (kg/s) eqn. 5	b (kg/s) eqn. 6
Natural frequency	18.9	0.0227	0.000407	0.0179	7583	0.538	0.470	
Resonant frequency	19.0				7583			12.685

Results are presented in Table 2. The measured value of mass is interesting since, at 0.538 kg, it is 26% lower than the nominal value for this structure given by Hallauer and Devenport (2006). This is particularly significant since their value ignored the

contribution from the two beams and thus should be an underestimate. The uncertainty in the present result (see appendix) is only 0.33 kg (6%), and cannot account for discrepancy. It seems probable therefore that the value given by Hallauer and Devenport (2006) is an overestimate, and should be revised.

The two measured values of the damping constant appear wildly inconsistent until one examines the uncertainty estimates (calculated in the appendix). Using the dynamic flexibility at the natural frequency and Equation (5) results in an uncertainty of 0.065 kg/s, about 14% of the measured value. This method therefore appears to result in a useful estimate of the damping. Using the measured resonant frequency and Equation (6), however, results in an uncertainty of some 13 kg/s, actually larger than the measured value. The uncertainty is dominated by the uncertainty in the frequency measurement of 0.1 Hz, see Table 6. The approach of inferring the damping from a measurement of resonant frequency, as compared to the natural frequency, is clearly not practical for this type of structure.

4. CONCLUSIONS

An experiment has been performed to determine the parameters governing the motion of a single-degree-of-freedom structural system by measuring the response of the structure to sinusoidal forcing. Measurements at very low frequency were made to determine the spring constant of the structure. Measurements of the natural frequency were used to determine the effective mass, m. To methods for determining the viscous damping, b, using measurements at the natural frequency and resonant frequency were compared. The following conclusions are drawn.

1. The structure has a spring constant of 7583±450 N/m, an effective mass of 0.538±0.33 kg and a viscous damping of 0.470±0.065 kg.
2. The present results confirm the nominal spring stiffness value given by Hallauer and Devenport (2006).
3. The effective mass of the structure is at least 26% less than the nominal value given by Hallauer and Devenport (2006). It is recommended that this nominal value be revised.
4. It is not possible to reliably infer the damping from a measurement of the resonant frequency as compared to the natural frequency, at least for the type of structure considered here.
5. A useful estimate of the damping can be obtained using the dynamic flexibility at the natural frequency.

REFERENCES

Hallauer W. L. Jr. and Devenport W. J., 2006, *AOE 3054 Experimental Methods Course Manual. Experiment 6 - Dynamic Response of a Beam Structure*, A.O.E. Department, Virginia Tech. Blacksburg VA.

Ogata, K., 1998, *System Dynamics*, 3rd edition, Prentice Hall.

APPENDIX: UNCERTAINTY CALCULATIONS

Uncertainties in measurements were calculated for 20:1 odds. Sources of uncertainty included the accuracy with which signal voltage amplitudes could be measured using the

oscilloscope, and the resolution of the counter used for frequency measurements. Specific uncertainties in these primary measurements are given in Section 2. To obtain uncertainties in results *R* derived from these measurements, uncertainties were combined using the root sum square equation,

$$\delta(R) = \sqrt{\left(\frac{\partial R}{\partial a}\delta(a)\right)^2 + \left(\frac{\partial R}{\partial b}\delta(b)\right)^2 + \left(\frac{\partial R}{\partial c}\delta(d)\right)^2 + \ldots} \qquad (7)$$

where *a*, *b*, *c*… are the measurements on which *R* depends. Partial derivatives were estimated numerically, the whole calculation being performed using a spreadsheet table. Calculations for the uncertainty in spring constant, *k*, mass, *m*, damping, *b*, determined from the dynamic flexibility at the natural frequency, and from the ratio of resonant to natural frequency, are given in Tables 3 to 6 below, respectively.

Table 3 Table for calculation of uncertainty in the spring constant, *k*.

				Perturbation	
		Quantity	**Uncertainty**	*a+da,b*	*a,b+db*
	Proximiter sensitivity (V/m)	4173.228		4173.228	4173.228
	Shaker calibration (N/V)	0.36342		0.36342	0.36342
	Input Variables				
a	Excitation voltage amplitude (V)	2	0.025	2.025	2
b	Response voltage amplitude (V)	0.4	0.025	0.4	0.425
	Intermediate results				
	Excitation force amplitude (N)	0.726839		0.735925	0.726839
	Response amplitude (m)	9.58E-05		9.58E-05	0.000102
	Final Result				
	Effective spring constant, *k* (N/m)	7583.164		7677.954	7137.096
			Change	94.78955	-446.068
	Uncertainty in spring constant (N/m)	456.0287			

Table 4 Table for calculation of uncertainty in the effective mass, *m*.

				Perturbation	
		Quantity	**Uncertainty**	*a+da,b*	*a,b+db*
	Input variables				
a	Effective Spring Constant	7583.164	456.0287	7583.164	8039.193
b	Natural Frequency (Hz)	18.9	0.1	19	18.9
	Intermediate results				
	Natural frequency (rads/s)	118.7522		119.3805	118.7522
	Final Result				
	Effective mass, *m* (kg)	0.537734		0.532088	0.570071
			Change	-0.00565	0.032338
	Uncertainty in mass (kg)	0.032827			

Table 5 Table for calculation of uncertainty in damping, *b*, when determined from the dynamic flexibility at the natural frequency

				Perturbation			
		Quantity	**Uncertainty**	*a+da,b,c,d*	*a,b+db,c,d*	*a,b,c+dc,d*	*a,b,c,d+dd*
	Proximiter sensitivity (V/m)	4173.228		4173.228	4173.228	4173.228	4173.228
	Shaker calibration (N/V)	0.36342		0.36342	0.36342	0.36342	0.36342
	Input Variables						
a	Excitation voltage amplitude (V)	0.0625	0.005	0.0675	0.0625	0.0625	0.0625
b	Response voltage amplitude (V)	1.7	0.2	1.7	1.9	1.7	1.7
c	Effective Spring Constant (N/m)	7583.164	456.0287	7583.164	7583.164	8039.193	7583.164
d	Effective Mass (kg)	0.537734	0.032827	0.537734	0.537734	0.537734	0.57056
	Intermediate results						
	Excitation force amplitude (N)	0.022714		0.024531	0.022714	0.022714	0.022714
	Response amplitude (m)	0.000407		0.000407	0.000455	0.000407	0.000407
	Dynamic flexibility, *d* (m/N)	0.017934		0.016606	0.020044	0.017934	0.017934
	Final Result						
	Viscous damping, *b* (kg/s)	0.469537		0.5071	0.420112	0.456025	0.483657
			Change	0.037563	-0.04942	-0.01351	0.01412
	Uncertainty in damping (kg/s)	0.065083					

Table 6 Table for calculation in damping, *b*, when determined from the ratio of the resonant and natural frequencies.

				Perturbation		
		Quantity	**Uncertainty**	*a+da,b,c*	*a,b+db,c*	*a,b,c+dc*
	Primary measurements					
a	Natural Frequency (Hz)	18.9	0.1	19	18.9	18.9
b	Resonant Frequency (Hz)	19	0.1	19	19.1	19
c	Effective Spring Constant (N/m)	7583.164	456.0287	7583.164	7583.164	8039.193
	Intermediate results					
	Frequency ratio	1.005291		1	1.010582	1.005291
	Final Result					
	Viscous damping, *b* (kg/s)	12.68522		0	17.96326	13.06108
			Change	-12.6852	5.278042	0.375857
	Uncertainty in damping (kg/s)	13.75312				

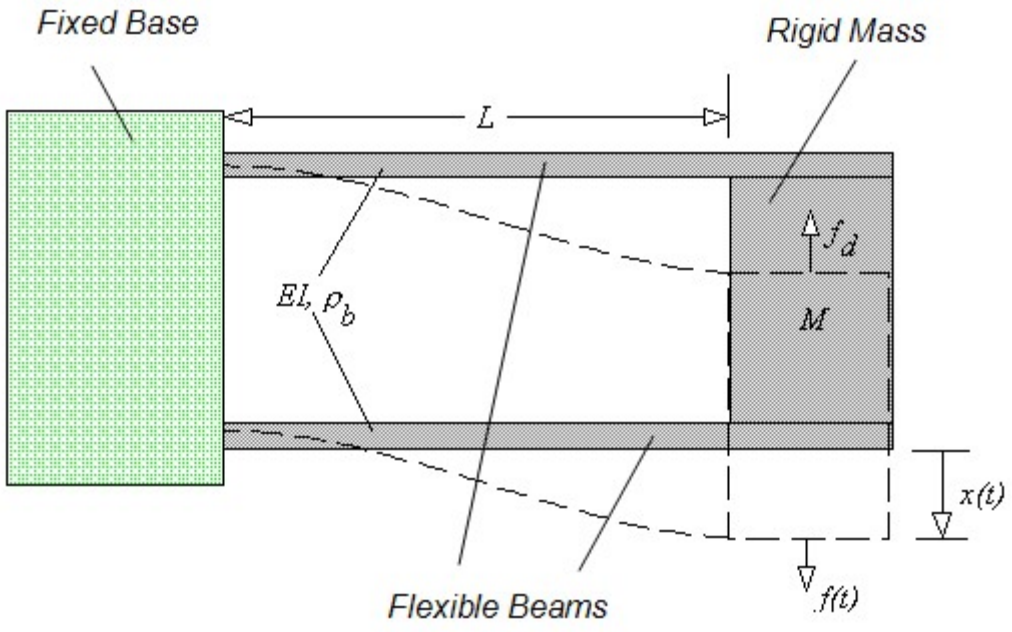

Figure 1. Diagram of the beam structure. Adapted from Hallauer and Devenport (2006).

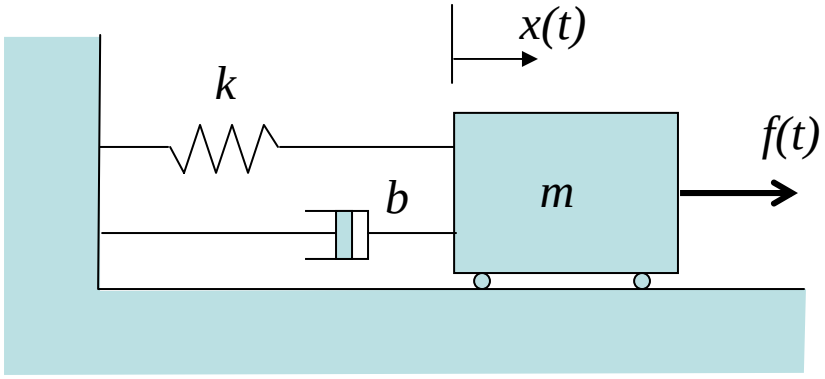

Figure 2. Idealized mechanical system equivalent to the beam structure in Figure 1.

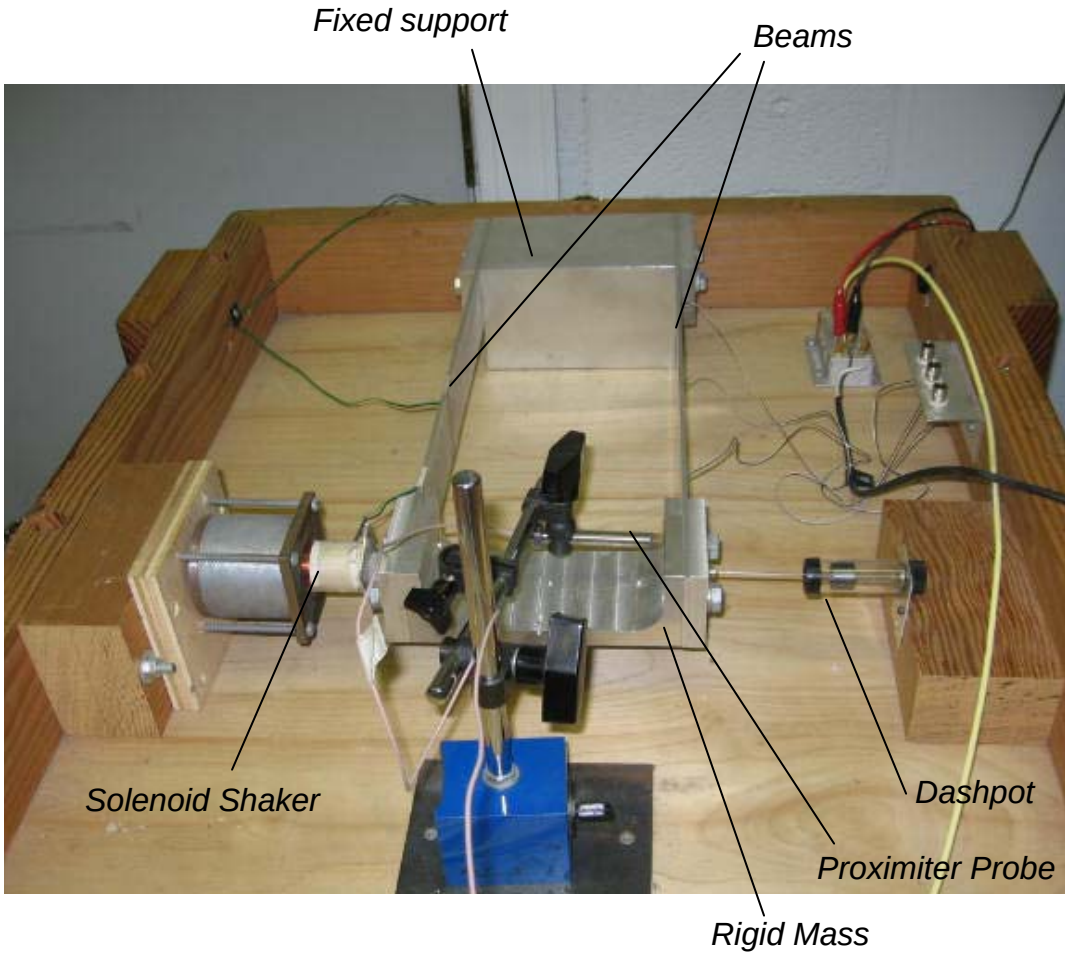

Figure 3. Photograph of the beam structure.

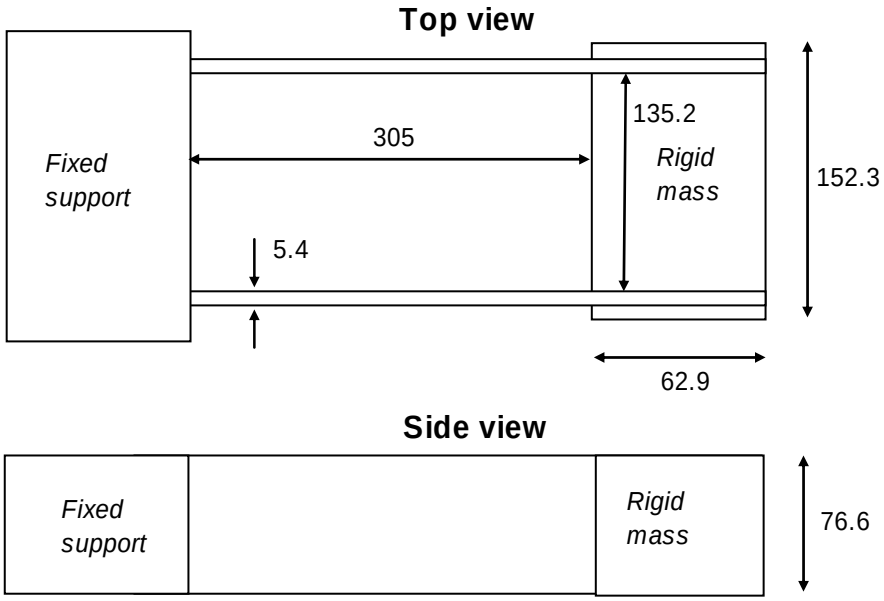

Figure 4. Beam structure dimensions (in mm).

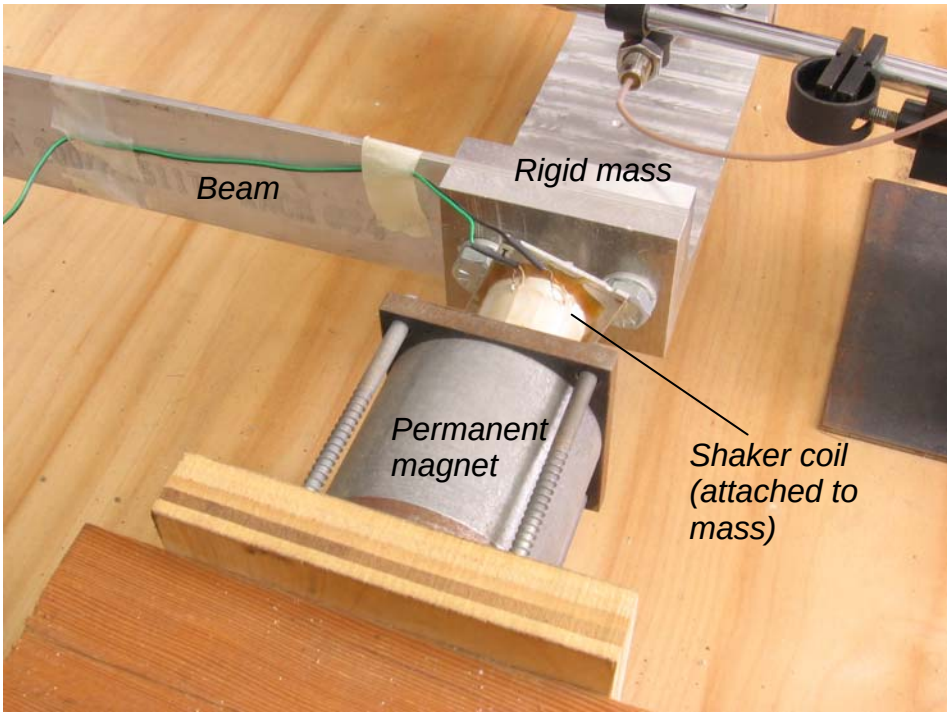

Figure 5. Detail showing the shaker and rigid mass.

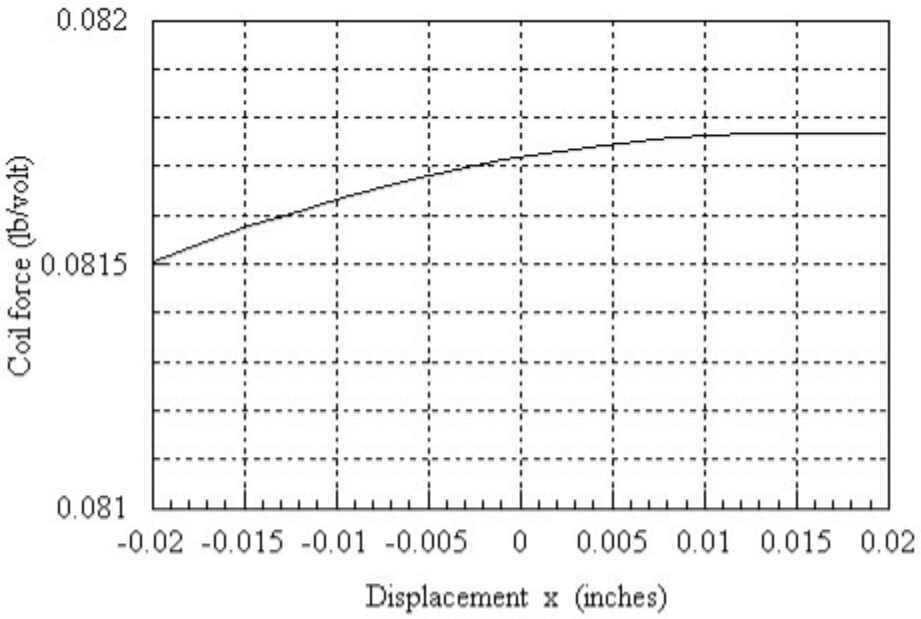

Figure 6. Shaker calibration. From Hallauer and Devenport (2006).

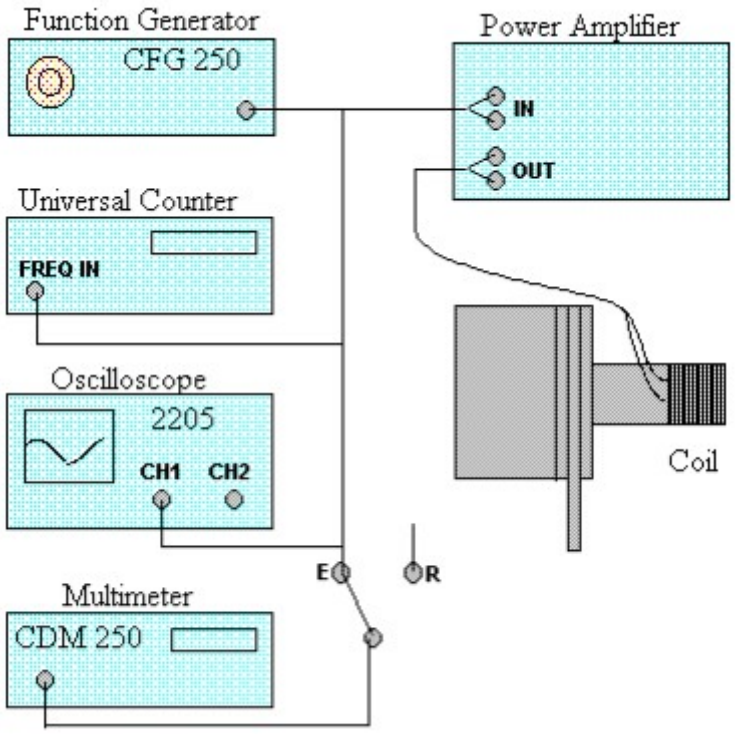

Figure 7. Schematic of the excitation system. From Hallauer and Devenport (2006).

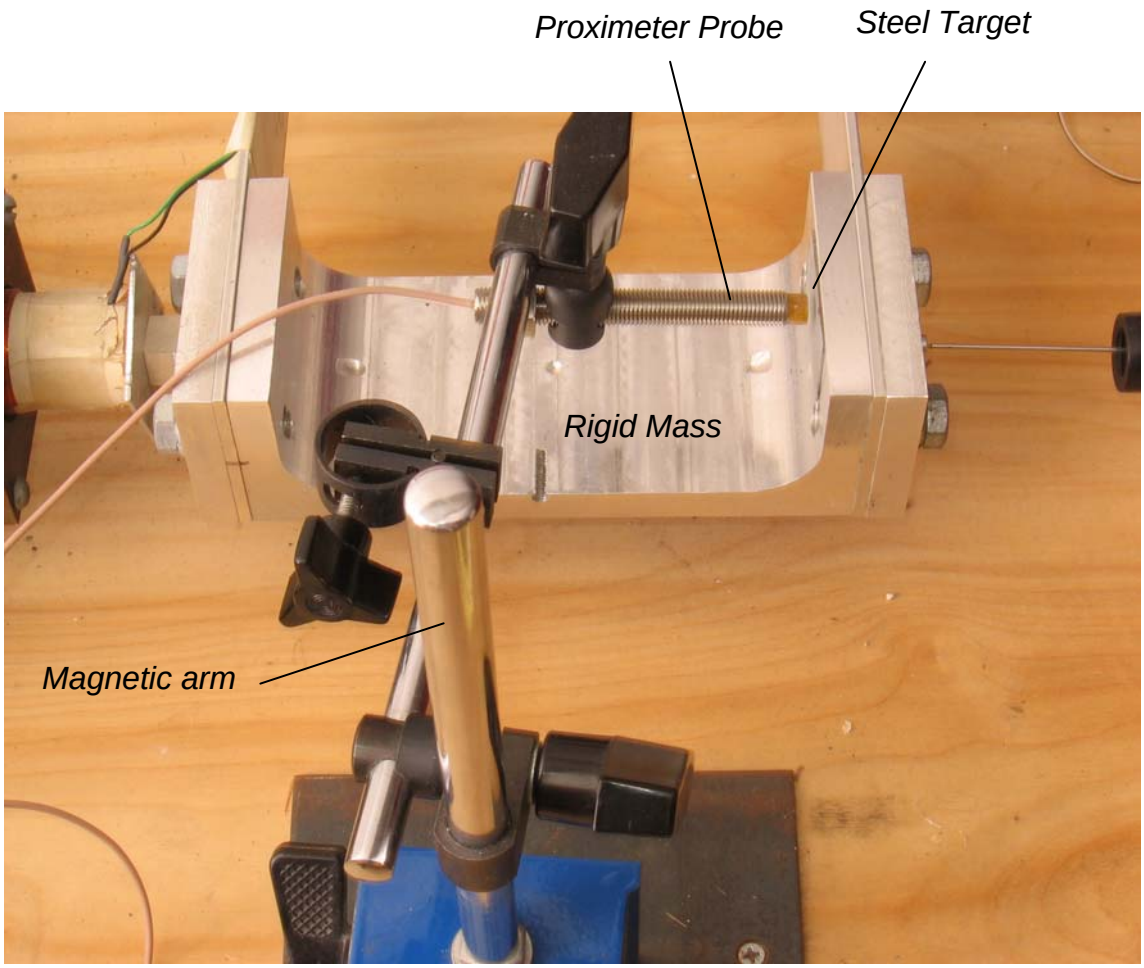

Figure 8. Detail showing the proximeter probe.

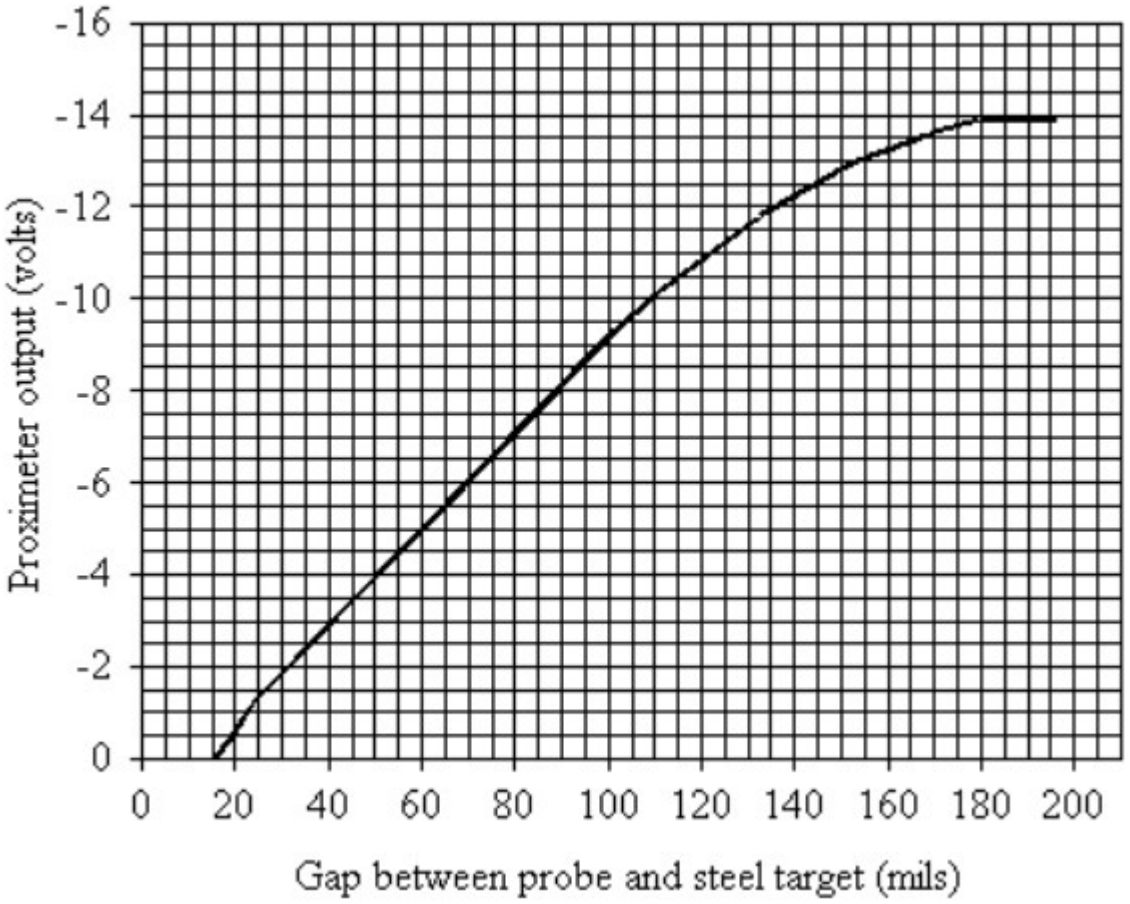

Figure 9. Proximeter calibration. From Hallauer and Devenport (2006).

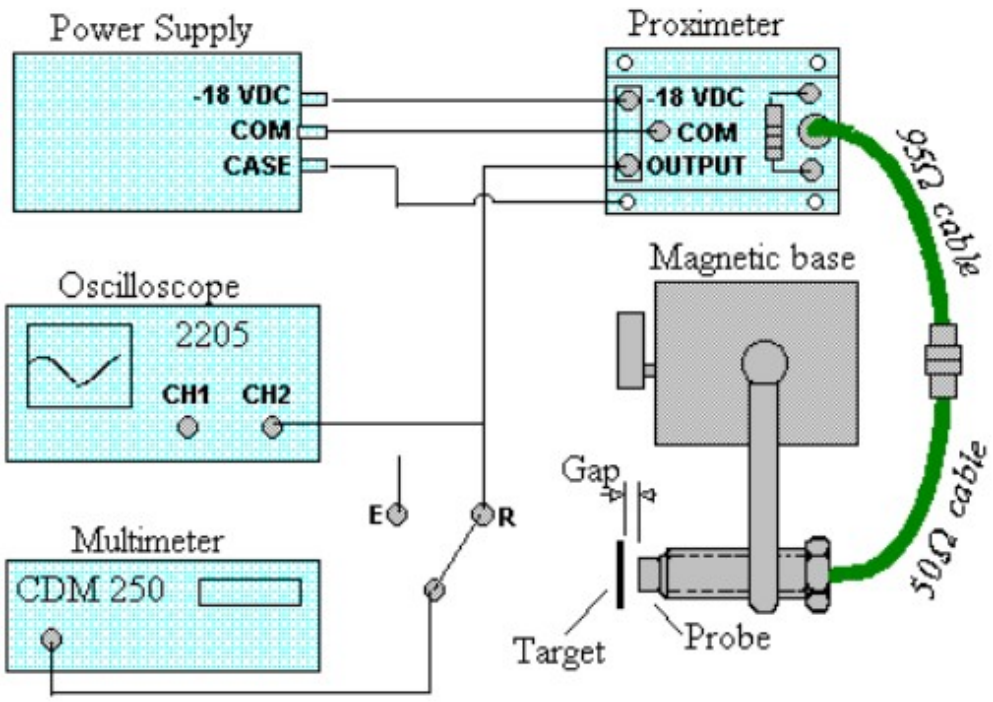

Figure 10. Schematic of the response system. From Hallauer and Devenport (2006).

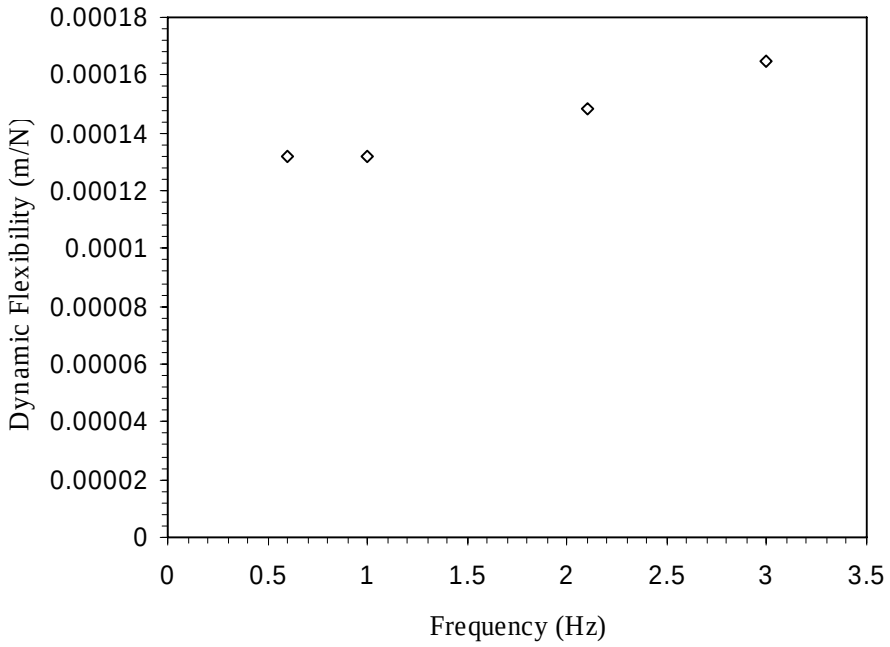

Figure 11. Dynamic flexibility of the structure at low frequencies.